

The composition and structure of the ubiquitous hydrocarbon contamination on van der Waals materials

András Pálincás^{1*}, György Kálvin¹, Péter Vancsó¹, Konrád Kandrai¹, Márton Szendrő¹, Gergely Németh², Miklós Németh³, Áron Pekker², József S. Pap³, Péter Petrik¹, Katalin Kamarás², Levente Tapasztó¹ and Péter Nemes-Incze^{1*}

¹Centre for Energy Research, Institute of Technical Physics and Materials Science, 1121 Budapest, Hungary

²Wigner Research Centre for Physics, 1121 Budapest, Hungary

³Centre for Energy Research, Institute for Energy Security and Environmental Safety, 1121 Budapest, Hungary

*corresponding authors: andras.palinkas@ek-cer.hu, nemes.incze.peter@ek-cer.hu

Abstract

The behavior of single layer van der Waals (vdW) materials is profoundly influenced by the immediate atomic environment at their surface, a prime example being the myriad of emergent properties in artificial heterostructures. Equally significant are adsorbates deposited onto their surface from ambient. While vdW interfaces are well understood, our knowledge regarding the atmospheric contamination is severely limited, even after the last decades of intense research in the field. Here we show that the common ambient contamination on the surface of: graphene, graphite, hBN and MoS₂ is composed of a self-organized molecular layer, which forms during a few days of ambient exposure. Using low-temperature STM measurements we image the atomic structure of this adlayer and in combination with infrared spectroscopy identify the contaminant molecules as normal alkanes with lengths of 20-26 carbon atoms. Through its ability to self-organize, the alkane layer displaces the manifold other airborne contaminant species, capping the surface of vdW materials and possibly dominating their interaction with the environment.

Introduction

Layered van der Waals materials have gained special interest in the last decade because many of them can be exfoliated down to single unit cell thickness. As the thickness decreases, surface effects become more pronounced; hence, both environmental adsorbates and substrates can substantially influence their properties¹. In the manufacturing of stacked van der Waals heterostructures, surface contamination may be one of the obstacles, which counteract the adhesion between the layers and thus limit the achievable configurations². Many experimental investigations and practical uses of vdW materials take place under ambient conditions, making surface contamination inevitable. To this day our knowledge is very limited about the components of such contamination, e.g., the main chemical elements; usually it is only described as ‘some hydrocarbon and adsorbed water’³. In recent years it was pointed out that the intrinsic nature of the materials’ surface could be totally hindered by contaminants, for example in the case of wetting properties^{4,5}.

During the last decade several groups reported 1D ordered structures on the surface of graphitic materials⁶⁻¹⁷, e.g. parallel stripes with 4-6 nm period, and suggested explanations for the stripe structure as the organized adsorption of molecules. First, Lu et al.^{6,7} proposed that the stripes can be built up from a self-assembled layer of molecular nitrogen, later a monolayer of organic chain-like molecules was also suggested^{14,15}. Despite the large number of observations⁶⁻¹⁷ there is no consensus on the chemical composition, nor the origin of the molecular layer. It is suggested in many of these reports that the stripe structure possibly follows the zigzag or the armchair direction of the surface’s hexagonal lattice. Gallagher et al. directly proved that the stripes are parallel to the armchair direction of the topmost graphene layer^{13,14}. Furthermore, it was also reported that, although the stripes can maintain their direction over several microns, 60° reorientation of the stripes can occur within the same crystal grains^{9,13,16}. Gallagher et al.¹³ proposed that a contamination layer could be the cause for the widely reported anisotropic friction on graphene and hBN, but the nature of the molecules forming the ordered surface cover could not be determined. Many groups reported anisotropic friction domains on various vdW materials: monolayer to few layer graphene^{13,14,18-21}, hexagonal boron nitride (hBN)¹³, molybdenum disulfide (MoS₂)^{12,21,22} and tungsten disulfide (WS₂)²³. In all these reports, the friction anisotropy exhibits common properties, such as a domain structure, C₂ rotation symmetry in each domain, 60° angles between the symmetry axes of adjacent domains, despite the differences in the chemical or mechanical properties of the host surface. In some studies the phenomenon was explained by periodic strain in the upmost layer¹⁸⁻²⁰, but no direct evidence

for such ripple formation was presented so far. As neither the detailed structure and chemical composition of the contamination layer^{13,14}, nor the presence of periodic strain ripples^{18–20} have been evidenced, the origin of such anisotropic frictional domains on vdW materials is still unclear^{21,24}.

Here, we show by surface sensitive methods (AFM, low-temperature STM, grazing angle IR, XPS and ellipsometry) that a self-organized layer of contaminant molecules grows on the clean surface of various vdW-materials exposed to ambient air. Furthermore, we have determined the subfamily of molecules responsible for the contamination layer: saturated, linear hydrocarbons in the form of normal alkanes, with carbon chain lengths from 20 to 26. We were also able to analyze the structure of the contaminant monolayer down to atomic resolution and controllably manipulate it by AFM.

Results

Parallel stripes of contaminants on vdW materials

Our Peak Force QNM® (hereinafter PF) AFM imaging of the flat terraces of van der Waals materials very often reveals parallel stripes with 3.0–5.2 nm period, similar to earlier reports by other groups^{6–17}. We have observed these parallel stripes on different surfaces: cleaved bulk graphite, exfoliated monolayer to few layer graphene on hBN or SiO₂, and 70–100 nm thick flakes of different vdW materials (graphite, hBN or MoS₂) supported on SiO₂. The stripes are observable in either the surface adhesion, deformation, dissipation, Young's modulus or in cases where the tip is sharp enough, in the topography channels (see Fig 1a). This stripe structure is not observed on freshly prepared samples and appears after a few days of ambient storage.

We observe the parallel stripes in PF topography maps recorded on flat terraces of three different bulk vdW materials (graphite, hBN, MoS₂), with the orientation of the stripes showing a domain-like behavior. We measured domains with a diameter from a few tens of nanometers to more than one hundred microns, having the same stripe orientation. Whereas on the border of the domains the orientation changes by 60°. In Fig 1a we present examples of these stripes within one such domain. The stripes are able to run through steps between terraces of highly oriented pyrolytic graphite (HOPG) (FigS1), to climb on bubbles formed on a vdW-heterostructure (FigS2) and to cross the border of an <1° graphene/hBN heterostructure (FigS3) without breaking. Similar stripes were commonly reported^{6–17}, but their molecular building blocks have not been identified, since their atomic structure could not be resolved. The

universality of their period among vdW substrates differing in chemical composition, lattice constant, thickness or mechanical strain fields (in case of bubbles) implicate a common, extrinsic origin.

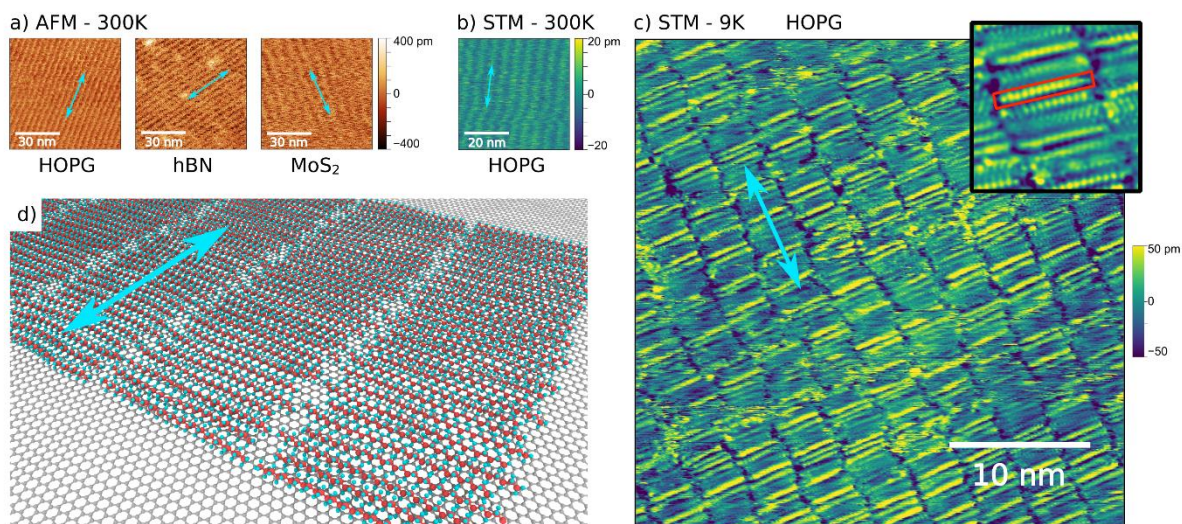


Fig1. Stripe patterns on vdW materials, due to ambient contamination. a) PeakForce QNM topography maps measured on the surface of bulk HOPG, hBN and MoS₂ crystal terraces showing parallel stripes. **b)** Room-temperature STM topography showing the smectic phase of the monolayer. **c)** Low-temperature (9 K) STM topography map showing the inner structure of the stripes: the single molecular building blocks and the superlattice along the stripes. Inset: 6×6 nm STM topography image showing the atomic scale structure of a molecular stripe. Single molecule is shown by the red rectangle. **d)** Schematic representation of the linear alkane molecules on a graphene surface. In all images light blue arrows are parallel to the direction of the stripes, identified by AFM.

Since the first reports from the early years of STM^{25–28}, a whole field emerged from the STM investigation of self-organizing molecular monolayers on graphite. This broad literature^{29–34} aides us in identifying the few possible molecules and to rule out a large variety of functional groups. We were able to achieve atomic resolution in low-temperature (9 K) STM images (Fig1c, Fig3a) on the contaminant molecular layer enabling us to resolve the inner structure of the stripes: the arrangement of the molecules, their precise length and lattice periodicity. The individual linear molecules lie side-by-side forming the stripes observed by AFM in the direction perpendicular to the molecular axis (light blue arrows in Fig1). The molecules in adjacent stripes tend to be shifted by a half-molecule width. We measured 3.27 ± 0.15 nm for the width of the stripes, which corresponds to an all-trans length of alkyl chains, having 24-25

carbon atoms³⁵. This width is in excellent agreement with the stripe width measured by AFM at room temperature (Fig1a), where we found 3.4 ± 0.3 nm on graphite and 3.7 ± 1 nm on hBN substrates.

In higher resolution STM images the linear molecules show a periodic modulation of the apparent height along their length marked by the red rectangle in the inset of Fig1c. Closer inspection of the contrast of adjacent molecules reveals a quasiperiodic modulation of the apparent height along the stripes, with a period of 4-6 molecules. Such periodicity originates from the interaction between the substrate and the molecules, resulting in a 1D superlattice along the stripe. The quasiperiodic nature of the superlattice can be seen over a 35×35 nm² area in Fig1c characterized by a period between 1.7 and 2.5 nm. These findings are in agreement with the low-temperature (70-80 K) STM images reported by Endo et al.³⁶ of an incommensurate crystalline phase of vapor-deposited normal alkanes on graphite. They found that the alkane monolayer is in a smectic phase at room-temperature, where only the stripes can be resolved, but the individual molecules cannot, because of their rapid translation parallel to their long axis^{36,37}. This is also the case for our own room-temperature STM measurements, where the atomic structure of the molecules cannot be resolved, leading to the image in Fig1b.

To image the molecular layer, a large tunneling resistance is needed, above $10\text{ G}\Omega$ ^{26,31,38}. In the case of Fig1c we used 20 pA tunneling current and 400 mV sample bias, resulting in $20\text{ G}\Omega$ tunneling resistance. Below 5-10 $\text{G}\Omega$ the tip starts perturbing the molecules and at parameters, which are normally used for graphene measurements (for example 500 mV, 100 pA) the tip penetrates the adlayer, resulting in only a noisy atomic resolution image of graphite²⁶.

Spectroscopic measurements

Infrared (IR) spectroscopy can aid in identifying the molecules, by measuring their unique vibrational signature. Furthermore, the presence of a large variety of functional groups, possibly attached to the molecule termini could be also identified. In the search for this signature, we used grazing-angle reflectance IR spectroscopy. After the measurement of one adsorbate-covered substrate, we measured a reference IR reflectance for each sample, by keeping it in the same position but exfoliating the top layers to reveal a pristine surface. In addition to the correction with the reference, a baseline removal was applied to obtain comparable spectra (see Fig2a). Because the large-scale shape and the position of the graphite terraces are not perfectly the same, this results in an observable graphite band (E_{1u} mode - 1583 cm^{-1}) in all the spectra³⁹.

This is the only notable feature in the spectra of the freshly cleaved HOPG. In the spectra of contaminant covered HOPG samples, we could identify the C-H stretching (three bands between 2850 to 2960 cm^{-1}) and scissoring modes (weak band at 1472 cm^{-1}), whereas other modes typical of functional groups (eg. -COOH, -OH, halides etc.) were absent.

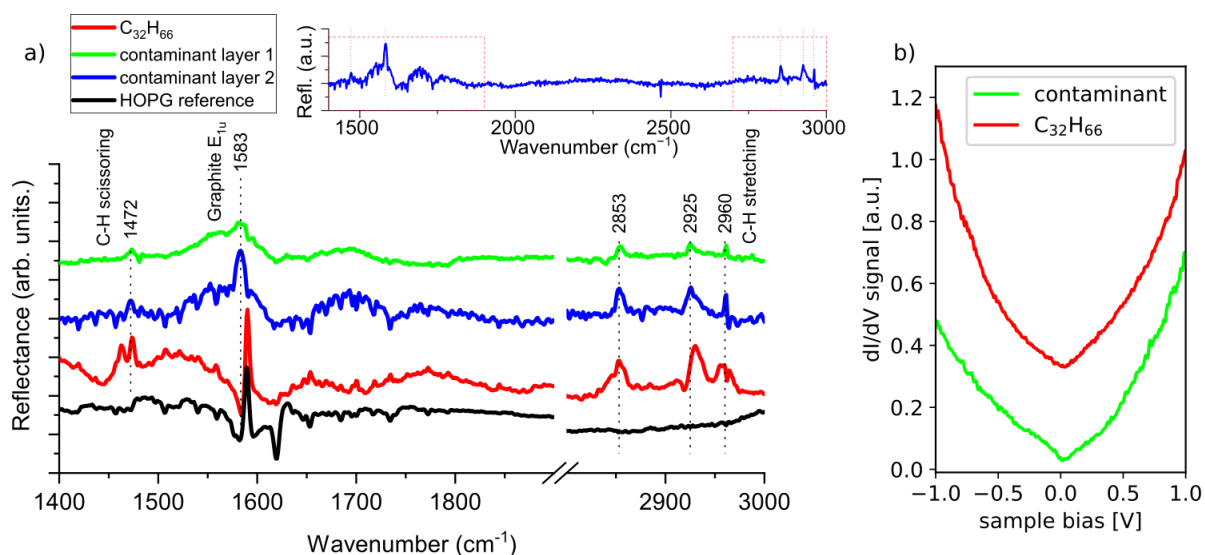


Fig2. Spectroscopy of the molecular contaminant layer. **a)** Grazing angle infrared spectra on differently covered graphite substrates, revealing the molecular vibrational modes of the adsorbates. The clean HOPG used as reference (black) shows only the E_{1u} graphite band at 1583 cm^{-1} , while the HOPG samples covered with adsorbates (blue, green) or vapor-deposited $C_{32}H_{66}$ layer show the C-H stretching and scissoring modes of alkanes. Inset: The spectrum of “contaminant layer 2” in the full wavenumber range. There are no other peaks aside from the ones presented in the main panel. **b)** STM measurement of the tunneling conductance (dI/dV) on top of the airborne contaminant layer and $C_{32}H_{66}$ (temperature 9 K). The spectra show the typical “V shaped” local density of states signal of graphite, with no sign of molecular states. The spectra are normalized to their respective tunneling conductance used for stabilization. Slight differences in the slope are due to different tips being used on the two samples. Both IR and dI/dV spectra are offset for clarity.

The measured IR spectra (blue and green on Fig2a) are consistent with normal alkanes as building blocks of the molecular contaminant layer. To further strengthen the case for this, or to disprove it, we have compared the spectra of the contaminant molecules to a monolayer of normal alkanes (dotriacontane, $C_{32}H_{66}$), deposited from the vapor phase onto a clean HOPG surface. In the spectrum of dotriacontane (red spectrum in Fig2a) we identified the same peaks as in the contaminant layer. However, the peak of the scissoring mode shows a splitting, which

could be due to the presence of double layers of dotriacontane⁴⁰. The contaminant layer shows only single peaks for both the stretching and scissoring modes, suggesting that it is mostly a monolayer.

Tunneling conductance (dI/dV) measurements further support the presence of normal alkanes. This quantity is proportional to the local density of states below the STM tip, at the energy associated with the sample bias. The dI/dV curves on both dotriacontane and the contaminant molecular layer show only the typical charge density of graphite in the energy range of ± 1 eV (Fig2b). This is expected for normal alkanes, since their lowest unoccupied and highest occupied molecular orbitals are more than 7 eV⁴¹ away from the graphite Fermi level. The observation that the dI/dV spectra show the “V shaped” graphite density of states further supports that the molecular layer is only one monolayer thick. Thicker molecular layers, without electronic states near the tip Fermi level, would render STM measurements on top of the molecules difficult, because the tip orbital cannot overlap with the p_z orbital of graphite. Stable STM imaging has been demonstrated in cases where there is an insulating monolayer in the tunnel junction, for alkanes²⁷ and a single layer of MoS_2 ⁴². Alongside the large tunneling resistance required for imaging, the featureless dI/dV signal of alkanes is another reason why this remarkable self-organized capping layer has gone unnoticed until now.

Atomic structure of the contaminant layer

In the following we show that comparison to $\text{C}_{32}\text{H}_{66}$ and *ab initio* modelling of the STM images further strengthens the case for normal alkanes forming the contaminant layer. In Fig3 we present higher magnification, low-temperature STM images of the contaminant (Fig3a) and the vapor-deposited dotriacontane (Fig3b) on graphite. Besides a more ordered arrangement in the artificially deposited, homogenous sample, the strong similarity to the contaminant layer is clear. In the contaminant layer (Fig3a), the stripes are formed by long alkyl chains stacked parallel to each other, with no sign of branching, unsaturated carbon-carbon bonds or benzene rings, similar to the case of dotriacontane (Fig3b). Changing the bias voltage between -1 to $+1$ V does not change the measured topography of the molecules and the relative contrast between neighboring molecules (see FigS4). This rules out many possible functional groups with higher local density of states and/or higher molecular polarizability^{28,30} (e.g. ethers, esters, amines, thiols, carboxylic acids, or $-\text{S}$, $-\text{I}$, $-\text{Br}$ chain terminations) which would have brighter contrast. The approximately rectangular structure (angle between the long axis of the molecule and the

stripe is $85\text{-}90^\circ$) in the self-organized layer means that functional groups which interlink by preferential hydrogen bonding²⁸ (eg. alcohols or surfactants) can also be discounted, since these prefer a different packing order. In the STM images alkyl chains with Cl heteroatoms could not be differentiated from normal alkanes⁴³. We ruled out that our alkyl chains would be terminated by Cl atoms based on XPS measurements, as the Cl 2p lines near 199 eV were absent from the spectra. We also did not detect any other ubiquitous elements (most notably N, S, Na, etc.), except for traces of oxygen with a concentration below 1% (see FigS5).

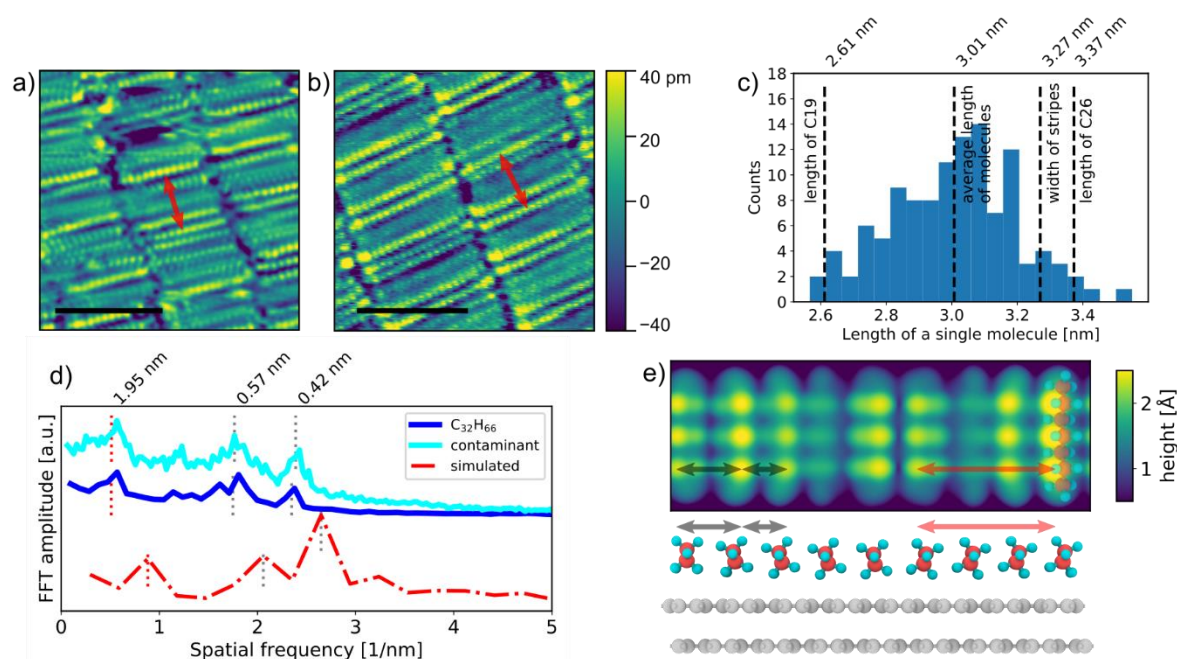


Fig3. Molecular structure from STM and *ab initio* calculations. High resolution STM images of the **a)** contaminant and **b)** $\text{C}_{32}\text{H}_{66}$ monolayer on HOPG at 9K (tip stabilization: 500 mV, 30 pA, scale bars: 4 nm). Red arrows show the quasiperiodic superlattice spacing. **c)** Distribution of the individual molecule lengths in the contaminant monolayer. **d)** 1D Fourier transform along the stripes of contaminant (cyan) and $\text{C}_{32}\text{H}_{66}$ (blue) topographic images showing the periodicities of the molecular spacing and quasiperiodic 1D superlattice. Red curve is the Fourier transform of **e)**, perpendicular to the molecule axis. Dashed lines mark the real space periodicities of the peaks as determined by Gaussian fitting. **e)** Top: calculated STM topographic image, at a bias voltage of 500 mV of C_7H_{16} alkanes on a bilayer graphene surface. The calculation cell is 3.41 nm long. Bottom: view along the molecular axis in the calculation cell, showing the equilibrium positions of the alkane chains. The apparent height of the alkanes in STM images is determined by the proximity of the hydrogen atoms to the STM tip and the position of the alkane chains on the graphite surface. Gray lines with arrows show the two interchain distances measurable by STM and in red the quasiperiodic superlattice length.

The dotriacontane ($C_{32}H_{66}$) monolayer self-organizes into the same striped structure as the contaminant layer, where the width of the stripe is equal to the length of the molecules, measured to be 4.27 ± 0.16 nm. This is in good agreement to the all-trans length of the molecule³⁵. The molecules lie parallel to the HOPG zigzag axis, the direction in which there is no significant contrast variation, whereas along the stripes (HOPG armchair direction) a quasiperiodic 1D superlattice can be observed, similarly to the contaminant layer (red arrows in Fig3a-b). The atomic period along a single $C_{32}H_{66}$ molecule is resolved as 16 dots, i.e., the hydrogens of every second carbon atom have the largest apparent height^{27,44}, but the atomic contrast is smeared periodically every 4-6 molecules, because the relative position to the underlying graphite lattice has a strong influence on the local charge density (see Fig3e). On the STM image of the contaminant molecules we could count 10-13 dots with 253 pm ($\pm 5\%$) spacing, in excellent agreement with the distance between alternate carbons in normal alkanes of 251 pm²⁷. Compared to dotriacontane, the contaminant layer has a larger variation of the individual molecular length of 2.57-3.55 nm, which corresponds to the all-trans length of normal alkanes with 20-26 carbon atoms. This is in agreement with the width of the stripes (3.27 ± 0.15 nm) measured from Fig1c.

In order to quantify the molecular spacing and quasiperiodic superlattice along the stripes, we calculate the Fourier transforms for each image line parallel to the stripes and average it for the entire image. We plot this 1D Fourier transform of the contaminant and $C_{32}H_{66}$ topographic images in Fig3d with cyan and blue lines, respectively. We can identify 3 peaks at the same positions on both Fourier signals. The peaks at 0.42 nm and 0.57 nm correspond to molecule-molecule distances. This duality is caused by the different atomic environment of the molecules above the graphite substrate, i.e. when the apparent height maximum is located on the hydrogens on the same side or the opposite sides of adjacent molecules (see black arrows in Fig3e). The peak at 1.95 nm corresponds to the quasiperiodic 1D superlattice in the heterogeneous contaminant alkane and dotriacontane layers. The periodicities appearing in the STM images are qualitatively reproduced by the 1D Fourier transform of a simulated STM image of edge-on oriented C_7H_{16} molecules on bilayer graphene (dash-dotted red line on Fig3d).

Simulations of alkanes on graphite

For a deeper understanding of the observed low-temperature ordering of the molecules, we modelled the arrangement of an alkane monolayer and simulated their STM image by *ab initio*

calculations. Relating to the arrangements of normal alkanes on graphite we shortly discuss two different cases from the literature: (1) the flat-on orientation²⁷ where the carbon zigzag plane of the alkanes is parallel to the graphite surface and (2) the edge-on orientation²⁸, where it is perpendicular (Fig3e). As we mentioned above, there is a vast literature of STM imaging of self-organized molecular monolayers (and in particular, alkanes) on graphite²⁵⁻³⁴, but the overwhelming majority of the experimental papers investigates the phenomenon at room-temperature, and at the solvent-graphite interface; therefore, they cannot be directly related to our case. Reports by Diama et al.³⁷ and Endo et al.³⁶ revealed temperature driven transitions between the edge-on and flat-on arrangement of vapor-deposited mid-length alkanes on graphite, which also underline the importance of the delicate balance between molecule-molecule and molecule-substrate interactions. The resolution of this detailed discussion is beyond the scope of the current paper; therefore, we will discuss both edge-on and flat-on cases.

The equilibrium spacing between the adjacent alkane molecules in their 3D solid form does not coincide with the graphite lattice which suggests the presence of a moiré period along the stripes. In our calculations we used the alkane-alkane distance on graphite from previous *ab initio* calculations by Yang et al⁴⁵, as 0.38 nm for edge-on oriented and as 0.45 nm for flat-on oriented molecules. Based on these values, in our DFT calculations, we modeled 9 (15) molecules in the edge-on (flat-on) orientation on graphite substrate in a 3.408 (6.816) nm long commensurate supercell perpendicular to the molecules. We found that in the case of the edge-on orientation the molecules have a slight rotation relative to the graphite surface, due to molecule-molecule interactions. The calculated STM image is mostly dominated by the hydrogens closest to the STM tip, thus after the rotation only one side of the molecule's hydrogen atoms are visible on every second C atom (see the rightmost C₇H₁₆ molecule on Fig3e) in good agreement with the experiments. It is known that besides geometrical effects, electronic effects (originated from the exact position of the alkane chain on the graphite substrate) can also affect the visibility of the molecules on an STM image⁴⁴. This feature appears in our STM simulated images as well, where molecules in the middle of the supercell have similar apparent height as the molecules at the ends of the supercell even though their hydrogen atoms are lower by 0.2 Å in the z-direction. The combined geometrical and electronic effects result in the variation of the apparent height of the molecules along the stripe, where 2-3 brighter molecules are followed by 1-2 molecules with lower contrast (Fig3e). This variability in the simulated STM images can explain the experimentally observed 1D quasiperiodic superlattice pattern in both the contaminant alkane layer, and the dotriacontane layer.

In order to compare more directly the simulated and measured periodicities, we performed the Fourier analysis of Fig3e perpendicular to the alkane chains. Similarly to the Fourier spectra of the measured molecular layers, we can identify 3 different peaks (periods) in the calculated image (red curve in Fig3d): 0.378 nm, 0.485 nm and 1.13 nm, which are in qualitative agreement with the experimentally measured Fourier components. The first two values correspond to the nearest-neighbor molecule distances, where the furthest hydrogens (0.485 nm) and the alkane-alkane chain separation (0.378 nm) dominate the contrast (grey arrows in Fig3e). The third value corresponds to the quasiperiodic modulation of the apparent height in the calculated STM image (red arrow), which is due to the rotation of the alkane chains and electronic effects discussed above. We can conclude that our *ab initio* model of alkane chains on a bilayer graphene surface reproduces the main characteristics of the measured STM images. The minor quantitative differences between the calculated and measured periods are the result of our initial choice of nearest-neighbor molecule distance in our calculations, which define the commensurate supercell. It is worth mentioning that the simulated STM image of a flat-on oriented alkane monolayer has qualitatively different features and does not describe our experimental data, in particular, it does not reproduce the observed superlattice (see FigS11).

Anisotropic friction domains

Measuring by contact mode AFM the contaminated vdW surfaces reveals a domain structure in the torsion (friction) signal, which cannot be linked to the features in the topography channel and is also present in atomically smooth regions (see FigS3 and FigS8b-c). The origin of these frictional domains^{12-14,18-23} was not conclusively clarified to date, which hinders the possibility to willingly manipulate or remove them. Our findings establish a direct causal link between the self-organized stripes of the adsorbed alkane layer and the friction anisotropy (Fig4a-b). We also demonstrate a precise and reliable method to nano-pattern (switch) the friction domains (Fig4c) on the flakes of vdW materials, regardless of their thickness.

In Fig4a we present a PF topography map on a monolayer graphene supported on hBN. A tripoint boundary with the three distinct orientations (rotated by 60°) of the stripes in the contaminant layer can be observed. The torsion signal of a subsequent contact mode AFM measurement (Fig4b) in the same region reveals the three distinct friction domains. The bright spots in Fig4a are additional amorphous adsorbates, which are easily swept out by the scanning AFM tip in contact mode. As we have shown above, the stripes parallel to the armchair direction

of the surface are formed by linear molecules which lie perpendicular to the stripes, namely the molecules are parallel to the zigzag direction. The triplicate nature of the friction domains is caused by the C3 symmetry of the three zigzag directions of the host surface. The parallel arrangement of the molecules with respect to a given zigzag direction in each domain gives a natural explanation to the commonly observed^{13,18,19} easy (zigzag) and hard (armchair) axes of the lateral force anisotropy. We also demonstrate the artificial creation of anisotropic friction domains by the vapor deposition of an alkane monolayer. The dotriacontane (C₃₂H₆₆) monolayer on HOPG, presented in Fig3b, displays the same domain-like anisotropic frictional characteristics as the naturally contaminated layer (see FigS7). By our knowledge, no other reliable, reproducible method was presented so far to controllably create the frictional anisotropy domains.

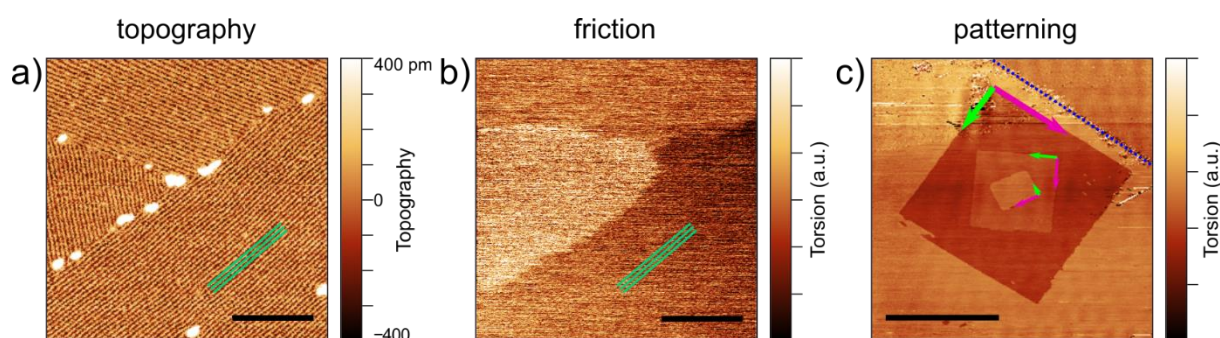


Fig4. Self-assembled alkane layer as the source of friction domains. **a)** PF topography image of a tripoint boundary of the stripes on graphene on hBN sample. **b)** Contact mode torsion signal on the same area as (a), revealing three distinct friction domains corresponding to the three differently oriented molecule domains. Scale bar on a-b: 100 nm **c)** Intentionally drawn nested, square-shaped friction domains generated by fast scanning parallel to the three zigzag directions of the substrate (pink arrows). The blue dotted line represents a zigzag-terminated edge of the thick (70 nm) hBN crystal on SiO₂, while pink and green arrows show the fast and slow scanning directions of the preceding drawing steps. Scale bar: 10 μ m.

It has to be noted, that the frictional difference between the domains decreases with increasing applied load (contact force setpoint)¹⁸, thus to get a better contrast, one should scan with low tip – sample force. On the contrary, scanning with sufficiently high normal load, we found that the friction domains can be switched by the AFM tip after reaching a threshold, and most importantly, by setting the fast scan direction parallel to the zigzag direction. In Fig4c we present the lateral force map on a 70 nm thick hBN crystal with deliberately patterned friction domains. A zigzag-oriented edge of the crystal (blue dotted line) marks the guideline for the fast scan orientation (indicated by a pink arrow) of the first 15 \times 15 μ m² area, followed by a

7.5×7.5 μm² and a 3×3 μm² area scans where the fast scan direction is changed by 60°(120°). The resulting nested square-shaped friction domains are presented in Fig4c. These patterns are stable for up to 6 months. On the other hand, by scanning with very high normal forces, the molecular overlayer can be oriented in any direction, but the formed domain pattern is unstable, it becomes patchy in a few minutes, as the molecules spontaneously rearrange to one of the three preferred zigzag directions of the substrate (see FigS10 in the case of thick MoS₂ and graphene on hBN).

The 60° direction change of alkyl backboned molecules by a scanning AFM tip on graphene was presented by Hong et al⁴⁶. Similarly to our findings, they stated that the fast scan direction needs to be parallel to the substrate zigzag axis to orient the adsorbed molecules in agreement with the broader literature of nanopatterning of directly deposited alkyl-backboned molecules⁴⁶⁻⁴⁹. Relating to the frictional anisotropy domains two previous publications have illustrated methods to switch them, but these findings are limited only to monolayers of graphene¹³ or WS₂²³. The first method, published by Gallagher et al.¹³, the final domain orientation on graphene was not predictable, but rather accidental and sometimes unstable. The method of Pang et al.²³ produced the desired and stable patterns, but the interpretation relies on the unproven hypothesis of ripple domains¹⁸. Here we demonstrated that the changeability of the domain structure is independent of the thickness of the host vdW material, which excludes their strain ripple origin.

Formation and removal of the alkane layer and friction domains

Despite the large number of experimental observations of naturally occurring friction domains in the literature, as far as we know there is no report where their evolution from the pristine surface is documented. First, we wanted to observe the formation of the contamination layer under ambient conditions. We could only find friction domains and ordered stripes structures on 4-5 day old samples, stored under lab conditions. We were unable to observe the formation of sub-monolayer self-organized domains or seeds by AFM even during 24 hours long measurements. From its fundamental design, AFM is probing the surface of the sample only locally and thus may not be able to fully track the evolution of the adsorbate layer. As a complementary technique, to monitor the layer formation, we used optical ellipsometry which is highly sensitive to the presence of adsorbed species over the whole sample surface. It was reported previously that within 40-60 minutes an unknown hydrocarbon layer builds up on the freshly cleaved (hydrophilic) surface of HOPG or graphene, which is responsible for the

generally observed hydrophobicity of the material^{4,5}. However, follow-up studies have shown that after 60 minutes the thickness of the contaminant layer did not reach a steady state, as evidenced by the further growth of the water contact angle^{50,51}. The growing contact angle due to hydrocarbon contamination was also reported for boron nitride nanotubes⁵², MoS₂^{53,54} and WS₂⁵⁴. We have performed similar, but longer-run (up to 2 months) ellipsometry measurements: we found that in spite of the fast build-up of a contaminant layer, the steady state is reached only after 10-14 days (FigS6). Based on the combination of AFM and ellipsometry investigations, we propose that in the first 40-60 minutes an unordered contamination layer grows on the surface (comprising water and diverse hydrocarbons) from higher partial-pressure molecules⁵⁵, which on a longer time scale are replaced/interchanged⁵⁶⁻⁵⁸ by normal alkanes, forming an ordered, stable (lower energy) capping layer. While the atmospheric abundance⁵⁹ and vapor pressure of alkanes⁶⁰ decreases with their length, the adsorption energy per carbon atom increases with the chain length^{58,61}. This results in the gradual replacement of smaller chain alkanes by longer ones on graphite surfaces⁵⁶⁻⁵⁸. Our findings indicate that this results in the growth of the layer comprising alkanes with 20-26 carbon atoms, also due to the limited atmospheric abundance of longer chain alkanes⁵⁹. It is worth to note that similar self-organized stripe structures were also observed to grow on a graphite surface from the liquid phase, particularly when using plastic syringes¹⁵.

Beyond the manipulation of the molecular lattice, and details of the growth dynamics, we show the controlled desorption of the contaminant layer through heat-treatment. We annealed the samples at 200 °C for 1 h at 3×10^{-2} mbar, which resulted in the disappearance of the friction anisotropy domains (see FigS9) and the stripe structure. Annealing at 200 °C for 1 h under ambient conditions also leads to the disappearance of domains and stripes, but results in less clean surfaces. This is due to the desorption of the molecular adlayer, as it was shown that monolayers of normal alkanes with 20-26 carbon atoms desorb from graphitic surfaces between 400 and 500 K^{62,63}. The removal of friction domains by annealing is in accordance with the previous findings of Choi et al.¹⁸.

Discussion

We have identified the chemical nature of the ubiquitous adsorbate layer forming on vdW crystals under ambient conditions. The building blocks of the adsorbate layer predominantly consist of mid-length normal alkanes, consisting of 20-26 carbon atoms. These molecules are very common in the environment: naturally occurring as a mineral (evenkite), present in the

cuticle of almost every living organism⁶⁴ and most importantly, they are also a product of crude oil refining. The presence of long chain alkanes has been shown to be part of the exhaust of internal combustion engines⁶⁵ and they are major components of lubricants and mineral oils. The molecules themselves have equilibrium vapor pressures in the order of 10^{-6} millibars (decreasing from 6.16×10^{-6} to 6.25×10^{-7} between $C_{20}H_{42}$ to $C_{26}H_{54}$, respectively). Our results show that they are responsible for the commonly observed stripe structures⁶⁻¹⁷ and friction anisotropy domains^{12-14,18-23} observed on the surfaces of different vdW-materials.

The observation that normal alkanes are present on graphene, graphite, MoS_2 and hBN suggests that these adsorbates could be universally present on vdW materials, at least on those characterized by a hexagonal lattice. Revealing their identity, is of key importance for understanding their origin, and their effects on the measured properties. Such crystalline alkane layers may themselves be interesting for some applications^{34,66,67}. One example can be the use of alkane capping as a barrier, to avoid ambient decomposition of air-sensitive 2D materials⁶⁸, or as gas barriers in conjunction with graphene layers⁶⁹.

Methods

Sample preparation

Graphite, few layer graphene, hBN or MoS_2 flakes were exfoliated onto Si/SiO₂ substrates with the standard scotch tape method. The freshly exfoliated samples did not show the striped structure, nor friction anisotropy domains. The samples were stored in standard square plastic box (Ted Pella Inc.) or plastic Petri dish (VWR International, LLC) in ambient laboratory conditions. After 4-5 days undisturbed storage the friction domains and the stripes could be observed by AFM. Although not strictly necessary, we found that an hour-long exposure to a 10^{-2} Torr vacuum makes the imaging of the stripes easier, possibly because the other volatile contaminations (e.g. water) are removed (see FigS1). The contaminant layer itself was even stable under UHV (5×10^{-11} Torr, 300K) for weeks inside the STM chamber.

For the IR, XPS and Ellipsometry measurements we used bulk (1×1×0.1 cm) HOPG (Structure Probe, Inc.). The crystals were mechanically cleaved to get a pristine surface. The presence of the molecular contamination and the stripe structure was always checked with AFM before IR, STM and XPS measurements.

Dotriacontane ($C_{32}H_{66}$, Sigma-Aldrich, purity: 97%) layer was deposited onto HOPG substrates from vapor phase. An appropriate charge of bulk dotriacontane grains was placed in a small glass dish. This small dish, together with the freshly cleaved HOPG was placed inside a larger Petri dish and sealed with the glass top. Vapor deposition of the dotriacontane layer occurred upon heating the cell for 30 minutes to 80 °C, above the melting point of $C_{32}H_{66}$, to reach high vapor pressure. After 30 minutes the substrate was taken out from the Petri dish and cooled down in ambient air. The glass Petri dish was cleaned with O/Ar plasma etching beforehand, in order to eliminate other organic compounds.

STM

STM measurements were done using an RHK PanScan Freedom microscope, at temperatures of 8.9 K and 300 K, in ultrahigh vacuum at a pressure better than 5×10^{-11} Torr. STM tips were prepared by mechanically cutting Pt/Ir (90%/10%) wire and were calibrated on a Au (111) surface. dI/dV measurements were recorded using a Lock-in amplifier, with a modulation amplitude of 10 mV at a frequency of 1267 Hz.

AFM

For the ambient AFM measurements, a Bruker Multimode 8 AFM with different piezo scanners were used. For the precise measurements of the stripe width (calibrated to the graphite lattice, with $\pm 5\%$ relative standard deviation) we used an 9159EVL scanner with max. $\sim 15 \times 15 \mu\text{m}$ scan area, while for the large scans an 9178JVL scanner (calibrated to commonly available $1 \times 1 \mu\text{m}$ calibration grid samples) with max. $\sim 150 \times 150 \mu\text{m}$ scan area. Both scanners were used in standard contact, lateral force and PeakForce QNM modes. We used very sharp (nominal tip radius: 2 nm, spring const: 0.4 N/m) Bruker ScanAsyst-Air AFM tips in PF. For the lateral force/contact mode measurements and for the reshaping of the friction domains we used $\mu\text{Masch HQ:NSC19/Al BS}$ (ntr: 8 nm, sc: 0.5 N/m) and Bruker DNP-10 D (ntr: 20 nm, sc: 0.06 N/m) alongside with the above mentioned ScanAsyst tips. However, the threshold setpoint (loading force) from where we could rearrange the friction domains showed variations and were typical for a given tip-sample combination, but in this manner the different probe types were not specifically distinguishable.

It is worth to note that in many PF measurements the stripes gave a better contrast in the adhesion or in the Young's modulus channels than directly in the topography as it was recognized by Woods et al. as well¹⁷.

We paid special attention to the distance measurement accuracy of our SPMs by calibrating the piezo scanners to the graphite atomic lattice (for the UHV STM and for the 9159EVL ambient AFM scanners). We always double-check and exclude the possibility of electronic or mechanic noise as the main source of the observed 1D periods by performing measurements on a given area with different scan sizes, scan rates, scan angles and setpoints.

***ab initio* calculations**

Electronic calculations were performed in the framework of density functional theory implemented in the VASP software package⁷⁰ using the plane wave basis set and projector augmented wave method⁷¹. We applied the generalized gradient approximation (GGA) with the parametrization of Perdew-Burke-Ernzerhof (PBE)⁷² with added van der Waals (vdW) corrections using the method of Grimme (DFT-D2)⁷³. The rectangular supercells consist of the graphite and the alkane molecules (C7) with period of $a=12.3$ Ang, $b=34.08$ Ang ($a=14.76$ Ang, $b=68.17$ Ang) for the edge-on (flat-on) orientations of the molecules, respectively. The supercells are constructed with a vacuum space of 18 \AA along the z direction. Atomic positions were relaxed using the conjugate-gradient method until the forces of the atoms were reduced to 0.01 eV/\AA and the cut-off energy for the plane-wave basis set was chosen to be 400 eV . The Brillouin zones were sampled with the Γ -centered K point grid of $6 \times 2 \times 1$ ($6 \times 1 \times 1$) for the edge-on (flat-on) geometries. Simulated STM images were obtained by using the Tersoff-Hamann approximation⁷⁴.

IR

The grazing angle reflectance IR spectra was measured by Bruker IFS 66/v vacuum FTIR spectrometer using a Harrick variable angle reflection accessory with 72° angle of incidence and 6 mm aperture. The HOPG samples were exposed to contaminants and measured with up to 6000 scans to increase signal to noise ratio. Reference scans were performed on the same HOPG after exfoliating the contaminated top layer. The extensive number of scans and the weak signal (0.05 - 0.1% change in transmission) necessitated the use of background correction. The instrumental artifacts produced broad spectral features which are distinguishable from molecular vibrations and easily removed by spline fitting.

XPS

Surface compositions of the samples were determined in a Kratos XSAM 800 XPS instrument. The samples were analyzed by using an unmonochromatized Al K-alpha source (1486.6 eV)

with a take off angle (relative to the surface) of 90° . Lens-defined selected-area XPS was used to analyze ≈ 6 mm spot on the sample surface. For the processing of data, the Kratos Vision 2 software provided by the manufacturer was used. The atomic ratio of the elements at the surface was calculated from the integral intensities of the XPS lines using sensitivity factors given by the manufacturer.

Ellipsometry

Ψ and Δ ellipsometry spectra have been measured by a Woollam M-2000DI rotating compensator ellipsometer at angles of incidence of 60° , 65° and 70° , where Ψ and Δ define the complex reflection coefficient $\rho = \tan(\Psi)\exp(i\Delta) = r_p / r_s$ (r_p and r_s denote the reflection coefficients for the polarizations that are parallel and perpendicular, respectively, to the plane of incidence). The measured spectra were evaluated using a two phase model of a substrate and an overlayer described by the Cauchy dispersion. The optical properties of the substrate were determined on a freshly cleaved sample. The wavelength range was limited to the visible region (450-750 nm) in which the reproducibility of Ψ is better than 0.02, whereas the total ranges of variation are approximately 0.1 and 0.2 for the short- and long-range measurements, respectively.

Acknowledgements

The work was conducted within the framework of the Topology in Nanomaterials Lendulet project, Grant No. LP2017-9/2/2017, with support from the European H2020 GrapheneCore3 Project No. 881603. Funding from the National Research, Development, and Innovation Office (NKFIH) in Hungary, through the Grants K-134258, K-131515, FK 125063 and Élvonal KKP 138144 are acknowledged.

Author contributions

APa and GK prepared the samples and performed the AFM measurements. APa, GK and KKa performed the STM investigation. MS and VP performed the ab initio calculations. GN, APe and KKam measured the IR spectra, while MN and JP performed the XPS measurements. PP was responsible for the ellipsometry measurements. LT contributed to data analysis and interpretation. PNI conceived and coordinated the project, with assistance from APa. APa and PNI wrote the manuscript, with input from all authors.

References:

1. Ryu, S. *et al.* Atmospheric oxygen binding and hole doping in deformed graphene on a SiO₂ substrate. *Nano Lett.* **10**, 4944–4951 (2010).
2. Kretinin, A. V. *et al.* Electronic Properties of Graphene Encapsulated with Different Two-Dimensional Atomic Crystals. *Nano Lett.* **14**, 3270–3276 (2014).
3. Khestanova, E., Guinea, F., Fumagalli, L., Geim, A. K. & Grigorieva, I. V. Universal shape and pressure inside bubbles appearing in van der Waals heterostructures. *Nat. Commun.* **7**, 12587 (2016).
4. Li, Z. *et al.* Effect of airborne contaminants on the wettability of supported graphene and graphite. *Nat. Mater.* **12**, 925–931 (2013).
5. Kozbial, A. *et al.* Understanding the intrinsic water wettability of graphite. *Carbon N. Y.* **74**, 218–225 (2014).
6. Lu, Y. H., Yang, C. W. & Hwang, I. S. Molecular layer of gaslike domains at a hydrophobic water interface observed by frequency-modulation atomic force microscopy. *Langmuir* **28**, 12691–12695 (2012).
7. Lu, Y. H., Yang, C. W., Fang, C. K., Ko, H. C. & Hwang, I. S. Interface-induced ordering of gas molecules confined in a small space. *Sci. Rep.* **4**, 1–8 (2014).
8. Haghighian, N. *et al.* Rippling of graphitic surfaces: a comparison between few-layer graphene and HOPG. *Phys. Chem. Chem. Phys.* **20**, 13322–13330 (2018).
9. Rastei, M. V., Heinrich, B. & Gallani, J. L. Puckering stick-slip friction induced by a sliding nanoscale contact. *Phys. Rev. Lett.* **111**, 1–5 (2013).
10. Wastl, D. S. *et al.* Observation of 4 nm pitch stripe domains formed by exposing graphene to ambient air. *ACS Nano* **7**, 10032–10037 (2013).
11. Wastl, D. S., Weymouth, A. J. & Giessibl, F. J. Atomically resolved graphitic surfaces in air by atomic force microscopy. *ACS Nano* **8**, 5233–5239 (2014).
12. Boland, M. J., Nasseri, M., Hunley, D. P., Ansary, A. & Strachan, D. R. Striped nanoscale friction and edge rigidity of MoS₂ layers. *RSC Adv.* **5**, 92165–92173 (2015).
13. Gallagher, P. *et al.* Switchable friction enabled by nanoscale self-assembly on graphene. *Nat. Commun.* **7**, 10745 (2016).
14. Gallagher, P. *et al.* Optical Imaging and Spectroscopic Characterization of Self-Assembled Environmental Adsorbates on Graphene. *Nano Lett.* **18**, 2603–2608 (2018).
15. Seibert, S., Klassen, S., Latus, A., Bechstein, R. & Kühnle, A. Origin of Ubiquitous Stripes at the Graphite–Water Interface. *Langmuir* **36**, 7789–7794 (2020).
16. Temiryazev, A., Frolov, A. & Temiryazeva, M. Atomic-force microscopy study of self-assembled atmospheric contamination on graphene and graphite surfaces. *Carbon N. Y.* **143**, 30–37 (2019).
17. Woods, C. R. *et al.* Macroscopic self-reorientation of interacting two-dimensional crystals. *Nat. Commun.* **7**, 1–5 (2016).
18. Choi, J. S. *et al.* Friction anisotropy-driven domain imaging on exfoliated monolayer graphene. *Science (80-.)*. **333**, 607–610 (2011).
19. Choi, J. S. *et al.* Facile characterization of ripple domains on exfoliated graphene. *Rev. Sci. Instrum.* **83**, 073905 (2012).
20. Choi, J. S. *et al.* Correlation between micrometer-scale ripple alignment and atomic-scale crystallographic orientation of monolayer graphene. *Sci. Rep.* **4**, 1–5 (2014).
21. Lee, J. H. *et al.* Universality of strain-induced anisotropic friction domains on 2D materials. *NPG Asia Mater.* **10**, 1069–1075 (2018).
22. Dagdeviren, O. E., Acikgoz, O., Grütter, P. & Baykara, M. Z. Direct imaging, three-dimensional interaction spectroscopy, and friction anisotropy of atomic-scale ripples on MoS₂. *npj 2D Mater. Appl.* **4**, 30 (2020).
23. Pang, F. *et al.* Strain-Engineered Rippling and Manipulation of Single-Layer WS₂ by Atomic Force Microscopy. *J. Phys. Chem. C* **125**, 8696–8703 (2021).
24. Lee, J. H., Cho, D.-H., Park, B. H. & Choi, J. S. Nanotribology of 2D materials and their macroscopic applications. *J. Phys. D. Appl. Phys.* **53**, 393001 (2020).
25. Foster, J. S. & Frommer, J. E. Imaging of liquid crystals using a tunnelling microscope. *Nature* **333**, 542–545 (1988).
26. Smith, D. P. E., Hörber, H., Gerber, C. & Binnig, G. Smectic Liquid Crystal Monolayers on Graphite Observed by Scanning Tunneling Microscopy. *Science (80-.)*. **245**, 43–45 (1989).
27. McGonigal, G. C., Bernhardt, R. H. & Thomson, D. J. Imaging alkane layers at the liquid/graphite interface with the scanning tunneling microscope. *Appl. Phys. Lett.* **57**, 28–30 (1990).
28. Rabe, J. P. & Buchholz, S. Commensurability and Mobility in Two-Dimensional Molecular Patterns on Graphite. *Science (80-.)*. **253**, 424–427 (1991).

29. Cyr, D. M., Venkataraman, B. & Flynn, G. W. STM Investigations of Organic Molecules Physisorbed at the Liquid–Solid Interface. *Chem. Mater.* **8**, 1600–1615 (1996).
30. Cyr, D. M., Venkataraman, B., Flynn, G. W., Black, A. & Whitesides, G. M. Functional Group Identification in Scanning Tunneling Microscopy of Molecular Adsorbates. *J. Phys. Chem.* **100**, 13747–13759 (1996).
31. Giancarlo, L. C. & Flynn, G. W. Scanning Tunneling and Atomic Force Microscopy Probes of Self-Assembled, Physisorbed Monolayers: Peeking at the Peaks. *Annu. Rev. Phys. Chem.* **49**, 297–336 (1998).
32. De Feyter, S. & De Schryver, F. C. Two-dimensional supramolecular self-assembly probed by scanning tunneling microscopy. *Chem. Soc. Rev.* **32**, 139–150 (2003).
33. De Feyter, S. & De Schryver, F. C. Self-Assembly at the Liquid/Solid Interface: STM Reveals. *J. Phys. Chem. B* **109**, 4290–4302 (2005).
34. Goronzy, D. P. *et al.* Supramolecular Assemblies on Surfaces: Nanopatterning, Functionality, and Reactivity. *ACS Nano* **12**, 7445–7481 (2018).
35. Craig, S. R., Hastie, G. P., Roberts, K. J. & Sherwood, J. N. Investigation into the structures of some normal alkanes within the homologous series C13H28 to C60H122 using high-resolution synchrotron X-ray powder diffraction. *J. Mater. Chem.* **4**, 977 (1994).
36. Endo, O. *et al.* Incommensurate crystalline phase of n -alkane monolayers on graphite (0001). *J. Phys. Chem. C* **115**, 5720–5725 (2011).
37. Diama, A. *et al.* Structure and phase transitions of monolayers of intermediate-length n -alkanes on graphite studied by neutron diffraction and molecular dynamics simulation. *J. Chem. Phys.* **131**, (2009).
38. Magonov, S. N. & Whangbo, M. *Surface Analysis with STM and AFM*. (VCH Publishers, 1996). doi:10.1002/9783527615117.
39. Nemanich, R. J., Lucovsky, G. & Solin, S. A. Infrared active optical vibrations of graphite. *Solid State Commun.* **23**, 117–120 (1977).
40. Yamamoto, M. *et al.* Softened CH stretching vibration of a long-chain n-alkane, n-C44H90, physisorbed on a Ag(111) surface: An infrared reflection absorption spectroscopic study. *J. Phys. Chem. B* **104**, 7370–7376 (2000).
41. Mao, J. X., Kroll, P. & Schug, K. A. Vacuum ultraviolet absorbance of alkanes: an experimental and theoretical investigation. *Struct. Chem.* **30**, 2217–2224 (2019).
42. Martinez-Castro, J. *et al.* Scanning Tunneling Microscopy of an Air Sensitive Dichalcogenide Through an Encapsulating Layer. *Nano Lett.* **18**, 6696–6702 (2018).
43. Chen, Q. *et al.* STM investigation of the dependence of alkane and alkane (C18H38, C19H40) derivatives self-assembly on molecular chemical structure on HOPG surface. *Surf. Sci.* **602**, 1256–1266 (2008).
44. Ilan, B., Florio, G. M., Hybertsen, M. S., Berne, B. J. & Flynn, G. W. Scanning tunneling microscopy images of alkane derivatives on graphite: role of electronic effects. *Nano Lett.* **8**, 3160–3165 (2008).
45. Yang, T., Berber, S., Liu, J.-F., Miller, G. P. & Tománek, D. Self-assembly of long chain alkanes and their derivatives on graphite. *J. Chem. Phys.* **128**, 124709 (2008).
46. Hong, L., Nishihara, T., Hijikata, Y., Miyauchi, Y. & Itami, K. Unidirectional molecular assembly alignment on graphene enabled by nanomechanical symmetry breaking. *Sci. Rep.* **8**, 2333 (2018).
47. Verstraete, L. & De Feyter, S. 2D Self-assembled molecular networks and on-surface reactivity under nanoscale lateral confinement. *Chem. Soc. Rev.* **50**, 5884–5897 (2021).
48. Verstraete, L., Greenwood, J., Hirsch, B. E. & De Feyter, S. Self-Assembly under Confinement: Nanocorrals for Understanding Fundamentals of 2D Crystallization. *ACS Nano* **10**, 10706–10715 (2016).
49. Takajo, D. *et al.* Replacement of molecules at liquid/solid interfaces. *Thin Solid Films* **438–439**, 428–432 (2003).
50. Kozbial, A. *et al.* Study on the surface energy of graphene by contact angle measurements. *Langmuir* **30**, (2014).
51. Andrew Kozbial. Understanding the Intrinsic Water Wettability of Graphite. (University of Pittsburgh, 2016).
52. Boinovich, L. B. *et al.* Origins of thermodynamically stable superhydrophobicity of boron nitride nanotubes coatings. *Langmuir* **28**, 1206–1216 (2012).
53. Kozbial, A., Gong, X., Liu, H. & Li, L. Understanding the Intrinsic Water Wettability of Molybdenum Disulfide (MoS₂). *Langmuir* **31**, 8429–8435 (2015).
54. Chow, P. K. *et al.* Wetting of mono and few-layered WS₂ and MoS₂ films supported on Si/SiO₂ substrates. *ACS Nano* **9**, 3023–3031 (2015).
55. Martinez-Martin, D. *et al.* Atmospheric contaminants on graphitic surfaces. *Carbon N. Y.* **61**, 33–39 (2013).
56. Xia, T. K. & Landman, U. Molecular Dynamics of Adsorption and Segregation from an Alkane Mixture.

- Science* (80-). **261**, 1310–1312 (1993).
57. Castro, M. A., Clarke, S. M., Inaba, A., Thomas, R. K. & Arnold, T. Preferential Adsorption from Binary Mixtures of Short Chain n -Alkanes; The Octane–Decane System. *J. Phys. Chem. B* **105**, 8577–8582 (2001).
 58. GROSZEK A.J. Selective adsorption at graphite/hydrocarbon interfaces. *Proc. R. Soc. London. A. Math. Phys. Sci.* **314**, 473–498 (1970).
 59. Andreou, G. & Rapsomanikis, S. Origins of n-alkanes, carbonyl compounds and molecular biomarkers in atmospheric fine and coarse particles of Athens, Greece. *Sci. Total Environ.* **407**, 5750–5760 (2009).
 60. Chickos, J. S. & Hanshaw, W. Vapor pressures and vaporization enthalpies of the n-alkanes from C 31 to C 38 at T = 298.15 K by correlation gas chromatography. *J. Chem. Eng. Data* **49**, 620–630 (2004).
 61. EVERETT, D. H. & FINDENEGG, G. H. Calorimetric Evidence for the Structure of Films adsorbed at the Solid/Liquid Interface: the Heats of Wetting of ‘Graphon’ by some n-Alkanes. *Nature* **223**, 52–53 (1969).
 62. Paserba, K. R. & Gellman, A. J. Kinetics and Energetics of Oligomer Desorption from Surfaces. *Phys. Rev. Lett.* **86**, 4338–4341 (2001).
 63. Paserba, K. R. & Gellman, A. J. Effects of conformational isomerism on the desorption kinetics of n-alkanes from graphite. *J. Chem. Phys.* **115**, 6737–6751 (2001).
 64. Cholakova, D. & Denkov, N. Rotator phases in alkane systems: In bulk, surface layers and micro/nano-confinements. *Adv. Colloid Interface Sci.* **269**, 7–42 (2019).
 65. Caumo, S., Bruns, R. E. & Vasconcellos, P. C. Variation of the Distribution of Atmospheric n-Alkanes Emitted by Different Fuels’ Combustion. *Atmosphere (Basel)*. **11**, 643 (2020).
 66. Yu, Y. *et al.* Epitaxially Self-Assembled Alkane Layers for Graphene Electronics. *Adv. Mater.* **29**, 1603925 (2017).
 67. Gobbi, M., Orgiu, E. & Samorì, P. When 2D Materials Meet Molecules: Opportunities and Challenges of Hybrid Organic/Inorganic van der Waals Heterostructures. *Adv. Mater.* **30**, 1–20 (2018).
 68. Bolognesi, M. *et al.* Epitaxial multilayers of alkanes on two-dimensional black phosphorus as passivating and electrically insulating nanostructures. *Nanoscale* **11**, 17252–17261 (2019).
 69. Kim, Y. J. *et al.* Two-Dimensional Stacked Composites of Self-Assembled Alkane Layers and Graphene for Transparent Gas Barrier Films with Low Permeability. *Nano Lett.* **22**, 286–293 (2022).
 70. Kresse, G. & Joubert, D. From ultrasoft pseudopotentials to the projector augmented-wave method. *Phys. Rev. B* **59**, 1758–1775 (1999).
 71. Blöchl, P. E. Projector augmented-wave method. *Phys. Rev. B* **50**, 17953–17979 (1994).
 72. Perdew, J. P., Burke, K. & Ernzerhof, M. Generalized Gradient Approximation Made Simple. *Phys. Rev. Lett.* **77**, 3865–3868 (1996).
 73. Grimme, S. Semiempirical GGA-type density functional constructed with a long-range dispersion correction. *J. Comput. Chem.* **27**, 1787–1799 (2006).
 74. Tersoff, J. & Hamann, D. R. Theory and application for the scanning tunneling microscope. *Phys. Rev. Lett.* **50**, 1998–2001 (1983).